Research Article

Yunhe Zou, Shufeng Tang*, Yuezheng Lan, Tingting Zhang, Shijie Guo

Investigation on the effects of the electrode type and thickness in Langevin ultrasonic transducers based on Euler–Bernoulli beam theory and finite element simulation

https://doi.org/10.1515/EHS-2023-0154
received November 05, 2023; accepted February 03, 2025

Abstract: Today, ultrasonic transducers are commonly used in various industries. Most of the ultrasonic transducers used in industry are of the longitudinal and piezoelectric type. With the development of the application of these transducers in recent years, the need for small-sized transducers has arisen. In the present research, the vibration behavior of the Langevin transducer with four piezoelectric layers is studied using the simple theory and finite element model. For this purpose, by extracting the governing equations and the corresponding boundary conditions, the characteristic equation of the system is derived, and the effect of various parameters on the natural frequency of the system is studied analytically. Through the finite element simulation analysis of the modal, natural frequencies, frequency response, and vibration mode shapes of the transducer are obtained. Finally, the optimal values are determined to achieve the minimum length for the transducer. The results show that in the case of using aluminum electrode layers, the minimum transducer length of 87.47 mm is achieved with the electrode thickness equivalent to 6 mm. It is about 6% shorter than the corresponding transducer length with a copper electrode. Aluminum electrodes in the Langevin transducer under study achieve the optimal size for the transducer.

Keywords: ultrasonic transducers, vibration characteristics, Euler, Bernoulli beam theory, optimum dimensions

*** Corresponding author: Shufeng Tang,** School of Mechanical Engineering, Inner Mongolia University of Technology, Hohhot, 010051, Inner Mongolia, China; Inner Mongolia Key Laboratory of Robotics and Intelligent Equipment Technology, Hohhot, 010051, Inner Mongolia, China, e-mail: tangshufeng@imut.edu.cn
Yunhe Zou: School of Mechanical Engineering, Inner Mongolia University of Technology, Hohhot, 010051, Inner Mongolia, China; Inner Mongolia Key Laboratory of Robotics and Intelligent Equipment Technology, Hohhot, 010051, Inner Mongolia, China, e-mail: zouyh@imut.edu.cn
Yuezheng Lan: School of Mechanical Engineering, Inner Mongolia University of Technology, Hohhot, 010051, Inner Mongolia, China; Inner Mongolia Key Laboratory of Robotics and Intelligent Equipment Technology, Hohhot, 010051, Inner Mongolia, China, e-mail: 1015201047@tju.edu.cn
Tingting Zhang: School of Mechanical Engineering, Inner Mongolia University of Technology, Hohhot, 010051, Inner Mongolia, China, e-mail: noname1885@jgsu.edu.cn
Shijie Guo: School of Mechanical Engineering, Inner Mongolia University of Technology, Hohhot, 010051, Inner Mongolia, China; Inner Mongolia Key Laboratory of Robotics and Intelligent Equipment Technology, Hohhot, 010051, Inner Mongolia, China, e-mail: sjguo@imut.edu.cn

1 Introduction

Ultrasonic vibration has been commonly used in various fields, such as cleaning surfaces, material separation, measuring residual stress, inspecting defects inside parts, and medicine (destruction of cancerous tumors, breaking stones created inside the body, etc.). Moreover, due to its undeniable and positive effects, it has been applied in many other fields, such as different production processes, including turning, drilling, welding, etc. The application of ultrasonic vibration in the processes of turning and drilling reduces the chipping forces and increases the smoothness of the surface (Madinei et al. 2013, Beirami et al. 2023). In metal forming processes, the use of ultrasonic vibration reduces the forming forces and increases the elasticity (Zhao et al. 2023, Yuan et al. 2023, Gu et al. 2024). Also, using vibrations in friction stir welding improves the welding quality and reduces the axial force of the tool during welding (Wang et al. 2023). Considering that the transducer is one of the main components in producing ultrasonic waves, whose main task is to convert electrical energy into mechanical energy, it has attracted the attention of many researchers.

Piezoelectricity and flexoelectricity are two mechanisms by which materials convert mechanical energy into electrical energy (Beni 2022a, b, Dehkordi et al. 2023). Piezoelectricity works best in specific crystals where stress

creates an electrical response, while flexoelectricity uses strain gradients (uneven deformation) to achieve the same effect and works in all materials (Samani and Beni 2018, Jahanghiry et al. 2016, Maleki and Mohammadi 2017, Minaei et al. 2021, Ghobadi et al. 2021). Piezoelectricity is a mature technology with many applications in sensors and actuators, while flexoelectricity is a newer field with potential for miniaturized devices and energy harvesting (Fallah and Arab Maleki 2021, Li et al. 2022a, 2024). The standard model of an ultrasonic transducer consists of several piezoelectric ceramic discs and two resonant rods (amplifiers). Piezoelectric materials in transducers have the property to act as sensors (Balali Dehkordi and Tadi Beni 2024, Tadi Beni 2016, Beni and Beni 2022). A piezoelectric material undergoes a length change due to an electric discharge or voltage change that is transmitted through the generator to the electrodes and from the electrodes to the piezoelectric plates (Piao and Kim 2017, Zhang et al. 2016). The length change causes longitudinal vibrations in the members. One of the most widely used types of transducers is Langevin transducers, which consist of four piezoelectric ceramic discs sandwiched between two cylindrical masses. Vjuginova (2019) pioneered the modeling and formulation of sandwich ultrasonic transducers, marking a seminal contribution in the field. Subsequently, researchers have introduced a plethora of design and modeling methodologies, including the equivalent electrical circuit, one-dimensional and three-dimensional analytical methods, matrix networks, and numerical techniques (Liu et al. 2024, Ma et al. 2024, Pérez-Sánchez et al. 2020). Li et al. (2022b) analyzed and designed piezoelectric transducers with a central mass in which the piezoceramics on both sides of the central mass have the same polarity and presented an electrical circuit model for the design of this type of transducer. Adachi et al. (2018) investigated the use of a Stumpy transducer to increase the mechanical quality factor of high-power transducers with high resonance frequency. Wellendorf et al. (2024) investigated the vibration behavior of Langevin transducers using a three-dimensional finite element model. The results of their study showed that due to the coupling of radial and longitudinal vibration modes, it is better to use transducers with a larger diameter. Sun et al. (2010) studied longitudinal vibration characteristics of cylindrical piezoelectric transducers with different electrode arrangements using the finite element method and experimental tests. Lu et al. (2017) proposed a new structure for Langevin ultrasonic transducers. Wu et al. (2018) presented new Langevin transducers based on the use of polymer materials. The results of their study showed that the transducers based on polymer materials have good performance. Zheng et al. (2023) introduced a double-armed cone-shaped flexoelectric transducer. Theoretical analysis was conducted on the vibration frequency of the tuning fork structure and the derivation of the bandwidth formula. Subsequently, simulation studies were carried out to investigate the electrode width and thickness of the cone structure. These simulations aimed to analyze various aspects of the transducer's performance, including output response, resonant frequency, bandwidth, and output impedance. Wang et al. (2019) presented new piezoelectric transducers and investigated their performance. They also investigated the static and dynamic efficiency of the transducers. In their study, after the construction of the transducer, the optimal working points of its performance, including the optimal values of axial and peripheral magnetic fields and torsional preload (to increase the range of torsional oscillation), were obtained. Karafi and Kamali (2021) investigated the frequency response of Langevin transducers using the electromechanical continuous medium model. They studied the effect of transverse vibrations, dielectric losses, and damping on the performance of these transducers.

Considering the growing demand for miniaturized high-power piezoelectric ultrasonic transducers in diverse fields like medical ultrasound, material processing, and nondestructive testing, this research presents a novel approach to optimizing their design. This study presents the optimization of high-power piezoelectric ultrasonic transducers, which is a very important task in many different industrial applications. Particularly, the detailed analysis of electrode thickness and type variations in the frame of optimizing Langevin transducers is the focus of this research work. In a word, the objective will be to find the length of the transducer while maintaining a constant natural frequency. This ensures that the transducer's performance remains consistent amidst electrode alterations, allowing for investigation into the stimulation of piezoelectric oscillatory displacement on transducer output using the energy method. Utilizing the simple theory, we derive the vibration equation for transducers with four piezoelectric layers, preserving their inherent properties. Subsequently, we explore the influence of diverse parameters on transducer performance through analytical solutions. Additionally, our research involves modeling and analysis of various horn shapes using finite element analysis, aiming to ascertain resonance frequency, vibration amplitude at the tool end, and mode shape alongside the horn profile. This endeavor seeks to innovate by developing a novel horn profile capable of generating heightened vibration amplitudes at the tool end, surpassing those achieved by conventional profile shapes.

2 Materials and methods

In this study, the effect of the thickness, type of electrodes, and material properties on the frequency response of an ultrasonic transducer is examined by analytical and finite element models. In this section, an analytical model based on the Euler–Bernoulli beam theory (Xie et al. 2024, Wang

et al. 2024) is first presented, followed by a detailed discussion of the finite element simulation.

2.1 Analytical modeling

Due to its wide application in the industry, in this research, the transducer having four piezoelectric layers with different dimensions and types is investigated. In this section, the governing vibration equation and boundary conditions are presented for the transducer with four piezoelectric layers, ignoring the damping effects. Figure 1 shows the Langevin transducer with four piezoelectric layers under extensive longitudinal loading $f(x, t)$ of forces P_0 and P_L at both ends. The thickness of the electrodes t_e is considered equal, and so is the thickness of the piezoelectric layers t_p. The Young's modulus and density are denoted by E and ρ. The subscripts b, e, p, and m denote backing, electrode, piezoelectric, and matching of the transducer, respectively.

In this study, we focused on analyzing structures with dimensions on the order of millimeters. While it is recognized that size effects can be significant in smaller-scale structures, particularly in the micro- and nano-scale range, it is important to consider the appropriateness of nonclassical theories such as couple stress theory about the scale and context of the study. Given the millimeter-scale dimensions of the structures under investigation, the effects typically observed at the micro- and nano-scale may not be as pronounced (Pourreza et al. 2021, Alijani 2022, Rezaee and Maleki 2015). Therefore, classical theories, which are well-established and widely accepted for macro-scale applications, were utilized for modeling the behavior of these structures.

By using Hamilton's principle and considering the simple theory (Rao 2019), the equations governing the behavior of the longitudinal vibrations of the transducer can be derived. According to the simple theory, when a bar undergoes deformation, its cross sections that were originally flat remain flat throughout the process. Additionally, except for the displacement component parallel to the bar's longitudinal axis, other displacement components within the bar are considered negligible. As the purpose of this research is to investigate the effect of the electrode characteristics on the natural frequencies of the system, damping has not been considered. For dynamic systems, Hamilton's principle is expressed as

$$\delta\int_{t_1}^{t_2}(T - U + W)\mathrm{d}t = 0, \tag{1}$$

where T, U, and W, respectively, represent kinetic energy, strain energy, and work done by external forces.

The strain energy caused by the axial strains of the system is obtained as follows:

$$\begin{aligned} U &= \frac{1}{2}\int_0^L\int_A E\left(\frac{\partial u}{\partial x}\right)^2 \mathrm{d}A\mathrm{d}x \\ &= \frac{1}{2}\int_0^{l_1} E_bA\left(\frac{\partial u_1}{\partial x}\right)^2 \mathrm{d}x + \frac{1}{2}\int_{l_1}^{l_2} E_eA\left(\frac{\partial u_2}{\partial x}\right)^2 \mathrm{d}x \\ &\quad + \frac{1}{2}\int_{l_2}^{l_3} E_pA\left(\frac{\partial u_3}{\partial x}\right)^2 \mathrm{d}x + \frac{1}{2}\int_{l_3}^{l_4} E_eA\left(\frac{\partial u_4}{\partial x}\right)^2 \mathrm{d}x \\ &\quad + \frac{1}{2}\int_{l_4}^{l_5} E_pA\left(\frac{\partial u_5}{\partial x}\right)^2 \mathrm{d}x + \frac{1}{2}\int_{l_5}^{l_6} E_pA\left(\frac{\partial u_6}{\partial x}\right)^2 \mathrm{d}x \\ &\quad + \frac{1}{2}\int_{l_6}^{l_7} E_eA\left(\frac{\partial u_7}{\partial x}\right)^2 \mathrm{d}x + \frac{1}{2}\int_{l_7}^{l_8} E_pA\left(\frac{\partial u_8}{\partial x}\right)^2 \mathrm{d}x \\ &\quad + \frac{1}{2}\int_{l_8}^{l_9} E_eA\left(\frac{\partial u_9}{\partial x}\right)^2 \mathrm{d}x + \frac{1}{2}\int_{l_9}^{l_{10}} E_mA\left(\frac{\partial u_{10}}{\partial x}\right)^2 \mathrm{d}x. \end{aligned} \tag{2}$$

Similarly, the kinetic energy due to the longitudinal motion of the system is obtained as

$$\begin{aligned} T &= \frac{1}{2}\int_0^L\int_A \rho\left(\frac{\partial u}{\partial t}\right)^2 \mathrm{d}A\mathrm{d}x \\ &= \frac{1}{2}\int_0^{l_1} \rho_bA\left(\frac{\partial u_1}{\partial t}\right)^2 \mathrm{d}x + \frac{1}{2}\int_{l_1}^{l_2} \rho_eA\left(\frac{\partial u_2}{\partial t}\right)^2 \mathrm{d}x \\ &\quad + \frac{1}{2}\int_{l_2}^{l_3} \rho_pA\left(\frac{\partial u_3}{\partial t}\right)^2 \mathrm{d}x + \frac{1}{2}\int_{l_3}^{l_4} \rho_eA\left(\frac{\partial u_4}{\partial t}\right)^2 \mathrm{d}x \\ &\quad + \frac{1}{2}\int_{l_4}^{l_5} \rho_pA\left(\frac{\partial u_5}{\partial t}\right)^2 \mathrm{d}x + \frac{1}{2}\int_{l_5}^{l_6} \rho_pA\left(\frac{\partial u_6}{\partial t}\right)^2 \mathrm{d}x \\ &\quad + \frac{1}{2}\int_{l_6}^{l_7} \rho_eA\left(\frac{\partial u_7}{\partial t}\right)^2 \mathrm{d}x + \frac{1}{2}\int_{l_7}^{l_8} \rho_pA\left(\frac{\partial u_8}{\partial t}\right)^2 \mathrm{d}x \\ &\quad + \frac{1}{2}\int_{l_8}^{l_9} \rho_eA\left(\frac{\partial u_9}{\partial t}\right)^2 \mathrm{d}x + \frac{1}{2}\int_{l_9}^{l_{10}} \rho_mA\left(\frac{\partial u_{10}}{\partial t}\right)^2 \mathrm{d}x. \end{aligned} \tag{3}$$

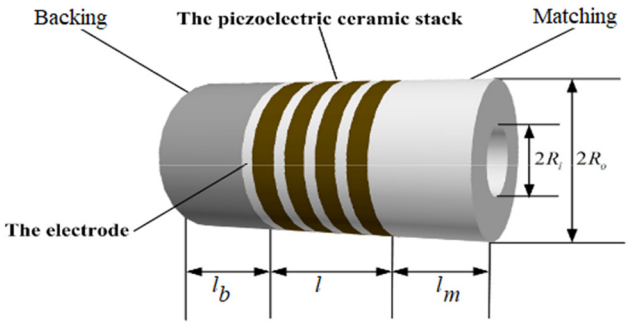

Figure 1: Dimensional model of the Langevin piezoelectric transducer. Source: Created by the authors.

Considering the external forces acting on the system, the work done by these forces is obtained as follows:

$$W = P_0 u(0, t) + P_L u(L, t) + \int_0^L f(x, t)u(x, t)\mathrm{d}x. \quad (4)$$

By using equations (2)–(4) and equation (1), and by applying part-by-part integration and performing some mathematical simplification operations, the governing equation of motion can be briefly obtained as

$$\rho(x)A(x)\frac{\partial^2 u}{\partial t^2} - E(x)A(x)\frac{\partial^2 u}{\partial x^2} = f(x, t), \quad (5)$$

where

$$\rho(x) = \sum_{j=1}^{9} \rho_j(x)\Delta_j H(x), \quad (6)$$

$$E(x) = \sum_{j=1}^{9} E_j(x)\Delta_j H(x), \quad (7)$$

$$A(x) = \sum_{j=1}^{9} A_j(x)\Delta_j H(x), \quad (8)$$

in which $H(x)$ represents the unit step function and

$$\Delta H_j(x) = H(x - L_{j+1}) - H(x - L_j), \quad j = 1, \ 2, \ldots, \ 9. \quad (9)$$

In the following, the analysis of the free vibrations of the transducer with four piezoelectric layers is discussed, and the relevant equations are extracted and presented along with the corresponding boundary conditions. To check the free vibrations, the external force is removed from equation (5), and the governing equation is rewritten as

$$c(x)\frac{\partial^2 u}{\partial t^2} = \frac{\partial^2 u}{\partial x^2}, \quad c(x) = \sqrt{\frac{\rho(x)}{E(x)}}, \quad (10)$$

where $c(x)$ is the sound velocity in the material.

Using the method of separating variables and assuming a harmonic response, the solution of the above equation can be considered as

$$u_j(x, t) = X_i(x)\mathrm{e}^{i\omega t}\Delta H_j(x). \quad (11)$$

As a result,

$$u(x, t) = \sum_{j=1}^{10} u_j(x, t)\Delta H_j(x) = \sum_{j=1}^{10} X_i(x)\mathrm{e}^{i\omega t}\Delta H_j(x). \quad (12)$$

Substituting the above relationships in equation (10), the mode shape in each part of the transducer is obtained as

$$X_j(x) = a_j \cos\frac{\omega}{c_j}(x - L_{j-1}) + b_j \sin\frac{\omega}{c_j}(x - L_{j-1}). \quad (13)$$

Considering the boundary conditions and obtaining the coefficients $a_j^{(k)}$ and $b_j^{(k)}$, the natural frequency ω is obtained, and finally, the general mode shape is obtained as

$$\begin{aligned}\phi_k(x) &= \sum_{j=1}^{10} X_j^{(k)} \cdot \Delta H_j(x) \\ &= \sum_{j=1}^{10}\left[a_j^{(k)}\cos\frac{\omega}{c_j}(x - L_{j-1}) + b_j^{(k)}\sin\frac{\omega}{c_j}(x - L_{j-1})\right] \\ &\quad \cdot \Delta H_j(x).\end{aligned} \quad (14)$$

Each of the components of the ultrasonic set, including the transducer (backing, piezoelectric layers, and matching) and the horn, is actually a free part that is placed together. Under the effect of harmonic oscillations of piezoelectric layers and according to the vibration properties of the continuous elastic body, they begin to vibrate in a balanced manner. There is no constraint limiting the movement between these components because the whole set can perform its oscillating task without being connected to the external environment. Only the effects caused by the stability of their momentum lead to the chain vibration of other elements, and the boundary conditions between them will be of the force type. This means that the boundary conditions of each component, such as the transducer, are considered to be two free ends. Since each of the components of the ultrasonic set is designed to vibrate at its natural frequency with the boundary condition $\partial u/\partial x = 0$, at the beginning and end of each component, the maximum vibrations (antinodes) occur, and nodes are formed between them. Clamping of the set is also done at the node point of a component, and therefore, the boundary condition of each component, such as a transducer, is considered as two free ends.

Using the boundary conditions obtained from the relations and the assumption of harmonic response, the boundary conditions can be rewritten as the following relations:

$$X'(0) = 0, \quad (15)$$

$$\begin{cases} A_i X_i'(L_i) = A_{i+1}X_{i+1}'(L_{i+1}) \\ X_i(L_i) = X_{i+1}(L_{i+1}) \end{cases}, \quad i = 1, \ 2, \ \ldots, \ 10. \quad (16)$$

By substituting equation (13) in the above boundary conditions, the coefficients a_j and b_j are calculated. Since all of the coefficients are calculated in terms of a_1, for simplification, it can be assumed to be equal to 1. From the last relation of the boundary conditions, an equation is obtained as follows, from which the natural frequency of the set can be obtained:

$$a_{10}\frac{\omega}{c_{10}}\sin\frac{\omega(L - L_0)}{c_{10}} + b_{10}\frac{\omega}{c_{10}}\cos\frac{\omega(L - L_0)}{c_{10}} = 0. \quad (17)$$

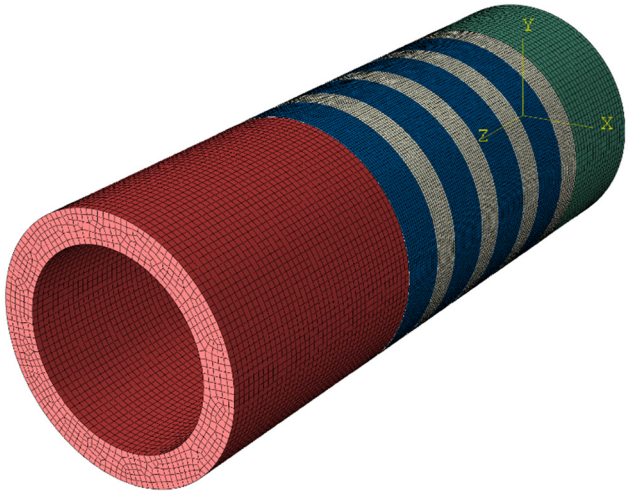

Figure 2: Finite element model of the Langevin transducer. Source: Created by the authors.

2.2 Finite element simulation

Finite element method (FEM) plays a crucial role in the design and analysis of complex systems (Esmaeili et al. 2023, 2021, Esmaeili and Andalibi 2019, Ghaderi et al. 2015), such as ultrasonic transducers, by providing detailed insights into their physical behavior under various conditions (Baghal et al. 2021, Pouraminian et al. 2024, Khosravi and Amjadian 2024, Khosravi et al. 2021). In the transducer's structure, the ceramic ring is pivotal for converting electrical energy into mechanical energy. Consequently, it is crucial to precisely calculate the values needed for the FEM model (Khosravi et al. 2025). The parameters of ceramic materials are calculated based on their linear electrical behavior. Linear electrical behavior and Hooke's law of ceramic materials are as follows:

$$D = \varepsilon E, \tag{18}$$

$$S = sT, \tag{19}$$

where D and ε are the electric charge density displacement and permittivity, and E stands for the electric field strength. S denotes strain, s is compliance under short-circuit conditions, and T is the stress tensor.

The finite element model of the transducer was created in ABAQUS software, as illustrated in Figure 2. The model employs C3D20 elements for conventional material parts and C3D20RE elements for the ceramic material. The parameters for the PZT8 ceramic material were calculated based on the theoretical framework described above, and the results are presented in Tables 1 and 2. The resonant frequency of the system is evaluated under free-standing conditions. This condition assessment provides a comprehensive understanding of the system's dynamic behavior. The analysis of the resonant frequency under free conditions allows for the determination of the system's natural frequency, unaffected by external interactions. The mode shape analysis further elucidates the deformation patterns and vibrational characteristics of the system, offering critical insights into its performance and stability. This comprehensive approach ensures a thorough understanding of the transducer's behavior in various operational scenarios. The boundary conditions were defined as in the study of Patel et al. (2021). The mesh used in this work is a hybrid with explicit solvers. In total, this mesh has 206,841 nodes. By this setup, a very accurate and fine examination of the system's behavior is achievable, where all of the material and structural dynamics will be well represented inside the finite element model. The PZT4 transducer material and its properties were modeled as presented in Tables 1 and 2, respectively. These tables are part of an extensive reference when defining material characteristics and operational parameters required to perform an accurate modeling and analysis of the performance of the transducer. Dynamic analysis, using finite element analysis, will extract the deformation of the transducer when a voltage is applied to the piezoelectric layers. This process allows for analyzing how the application of voltage influences the structural response of the transducer, providing information on its mechanical behavior under operation conditions.

Table 1: Mechanical specifications of different parts of the transducer

	Electrode	Matching	Piezoelectric	Backing
Young's modulus (GPa)	Cu: 130 Al: 70	210	67.4	72
Density (kg/m^3)	Cu: 8,960 Al: 2,700	7,850	7,600	2,700
Length (mm)	Cu: 0.3–2 Al: 2–10	45	5	43

Table 2: Material properties of the PZT4 piezoelectric material

Permittivity	Stiffness matrix (MPa)	Stress matrix (C/m^2)	Relative permittivity
8.854×10^4 F/m	$c_{11} = c_{22} = 13.9$, $c_{21} = 7.78$, $c_{31} = c_{32} = 7.43$, $c_{44} = 3.06$, $c_{55} = c_{66} = 2.56$	$e_{31} = -5.2$, $e_{33} = 15.9$, $e_{15} = 12.7$	$\varepsilon_{r11} = 1{,}472$, $\varepsilon_{r22} = 1{,}509$, $\varepsilon_{r33} = 1{,}280$

3 Results and discussion

In this section, the effects of changing the material as well as changing the thickness of the electrodes used in the transducer are investigated. In extracting the results, the properties of the parts, including backing, matching, and piezoelectric layers, are constant, and by changing the lengths of backing and matching, the natural frequency of the set is considered to be constant at 20 kHz.

It should be noted that the following results are extracted according to the values in Table 1. In order to examine the effect of different constraints on the natural frequencies of the transducer, the influence of the thickness of the electrode and piezoelectric layers on the first natural frequencies is shown in Figures 3 and 4. According to Figure 3, it can be seen that, in general, with the increase in the thickness of the electrode layers, the natural frequency decreases. By increasing the thickness of the piezoelectric layers from 10 to 50 mm, the first natural frequency is reduced for the cases of copper and aluminum electrodes by about 27 and 24%, respectively. Therefore, it can be concluded that the amount of frequency reduction for the copper electrode is greater than that of the aluminum electrode. In addition, the results demonstrate that due to the high elastic modulus of copper, under the same conditions, the frequency of the transducer with copper electrode layers is higher than the corresponding case of aluminum. Similar results can also be observed, as shown in Figure 4, for the effect of the thickness of the piezoelectric layer on the natural frequency values of the transducer. It can be seen that the use of copper electrodes increases the natural frequency values compared to the corresponding use of the aluminum electrodes, and this effect is more evident as the length of the piezoelectric layers increases. For instance, for piezoelectric layers with a thickness of 50 mm, the natural frequency of the transducer with the copper electrode is about 8.4% higher compared to the corresponding case of using the aluminum electrode. The differences in natural frequency trends between copper and aluminum electrodes can also be explained by their distinct material properties. The higher elastic modulus of copper results in greater stiffness, increasing the natural frequency but limiting size reduction. In contrast, aluminum's lower stiffness enables more effective optimization at the expense of a slightly lower natural frequency. Future studies could benefit from investigating these mechanisms in more detail, particularly by incorporating advanced modeling techniques to capture complex interactions between material properties and transducer performance.

Figure 5 shows the effect of backing length on the values of the first natural frequency. It can be seen that with the increase of the backing length, the natural frequency decreases, and the reduction rate of the natural

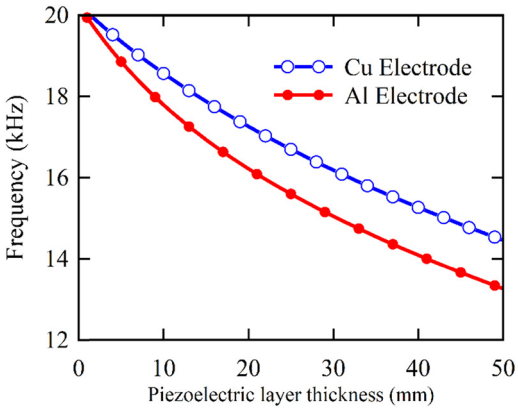

Figure 4: Influence of the piezoelectric thickness layer on the first natural frequency of the transducer. Source: Created by the authors.

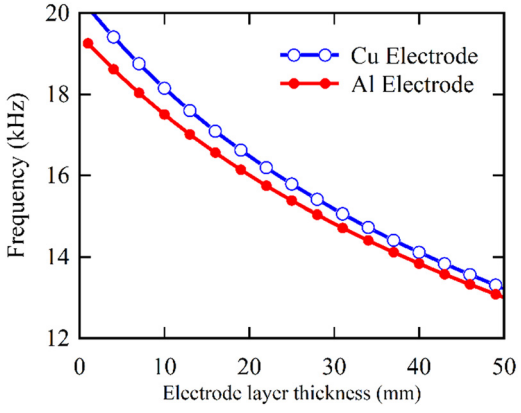

Figure 3: Influence of the electrode thickness on the first natural frequency of the transducer. Source: Created by the authors.

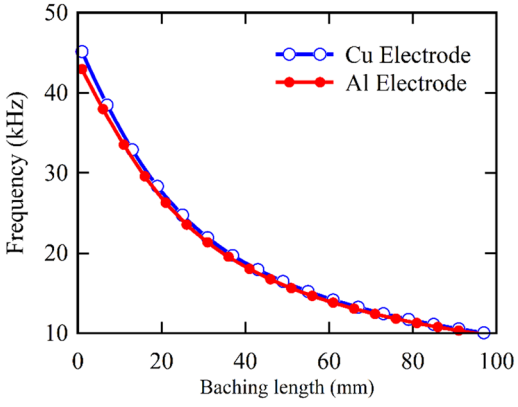

Figure 5: Effect of the backing length on the first natural frequency of the transducer. Source: Created by the authors.

Table 3: Suitable values of backing and matching lengths for different thicknesses of copper electrodes

No.	Frequency (kHz)	Overall transducer length (mm)	Thickness (mm)	Matching length (mm)	Backing length (mm)
1	20.020	94.57	0.3	57.42	15.95
2	20.019	94.71	0.5	56.88	15.83
3	20.046	94.15	0.7	55.81	15.54
4	20.038	94.00	0.9	55.08	15.32
5	20.109	93.93	1.1	54.36	15.17
6	20.020	93.88	1.3	53.74	14.94
7	20.014	93.68	1.5	52.92	14.76
8	20.000	93.67	1.7	52.28	14.59
9	19.987	93.39	1.9	51.48	14.31
10	20.001	93.07	2.0	50.83	14.24

frequency is less at high values of the backing length. In addition, the results show that for the backing length greater than 30 mm, the first natural frequency of the transducer is almost the same for both types of copper and aluminum electrodes. The observed reduction in natural frequency with increasing electrode thickness can be attributed to the added mass and reduced stiffness of the transducer system. This mass–stiffness interaction plays a critical role in determining the system's vibrational characteristics. Additionally, the superior performance of aluminum electrodes in minimizing transducer size is closely related to their lower elastic modulus, which allows for better vibration damping and material flexibility, leading to more compact designs.

Considering the fixed operating frequency of 20 kHz, appropriate values of backing and matching lengths are presented in Tables 3 and 4, considering the different thicknesses of copper and aluminum electrodes. According to the results, it can be seen that, in general, by increasing the thickness of the electrode layers, the lengths of the backing and matching parts decrease. Increasing the electrode thickness from 0.3 to 2.0 mm, the thickness of the backing and matching parts decreases by about 13 and 10%, respectively. In addition, the results display that for this increase in electrode thickness, the overall transducer length decreases by about 1.7%. The results shown in Table 3 demonstrate that the transducer length first increases by increasing the electrode thickness (from 0.3 to 0.5 mm). Then, by increasing the thickness from 0.5 to 0.7 mm, the transducer length decreases, and the minimum length is obtained for the copper electrode thickness equal to 2.0 mm.

However, such a result is not true for the aluminum electrode, and although the lengths of the backing and matching parts decrease with the increase of the electrode thickness, the overall transducer length does not follow this trend. The results obtained for the effect of the aluminum electrode thickness in Table 4 show that the transducer length first increases by increasing the electrode thickness (from 2 to 6 mm). Then, by increasing the thickness from 7 to 12 mm, the transducer length decreases. Based on the results presented in Table 4, it can be seen that the minimum transducer length is achieved for the thickness of the aluminum electrode layer equal to 6 mm, and its value is equal to 87.47 mm. These results show that the use of aluminum electrodes in the

Table 4: Suitable values of backing and matching lengths for different thicknesses of aluminum electrodes

No.	Frequency (kHz)	Overall transducer length (mm)	Thickness (mm)	Matching length (mm)	Backing length (mm)
1	20.043	92.49	2.0	50.4	14.09
2	19.999	91.37	3.0	46.44	12.93
3	20.017	90.36	4.0	42.48	11.88
4	20.025	89.54	5.0	38.79	10.75
5	20.065	87.47	6.0	34.02	9.45
6	20.046	89.29	7.0	31.54	8.75
7	19.987	88.96	8.0	29.66	8.30
8	19.984	88.45	9.0	25.45	7.0
9	20.085	88.06	10.0	21.96	6.1
10	20.007	93.26	12.0	20.06	5.2

Table 5: First three frequencies of the classical Langevin transducers

Frequency	Sun et al. (2010)	FEM (Sun et al. 2010)	Present work	Error (%)
First	55.66	55.65	53.68	3.52
Second	205.65	205.61	201.37	2.06
Third	269.71	269.81	257.89	4.42

Langevin transducer under investigation achieves the most optimal size for the transducer.

To validate the results presented in this research, the results of Sun et al. (2010) are used. Sun et al. (2010) investigated the vibration characteristics of the classical Langevin transducers using the numerical method and ATILA finite element software. Considering the geometry of Sun et al. (2010), the first three natural frequencies of the system are compared in Table 5. As can be seen, the maximum error is less than 5%. The cause of this error can be explained by different theories used as well as different methods of solving equations.

To examine the impact of mesh size on the vibration amplitude and resonant frequency of the ultrasonic transducer, a series of numerical simulations was conducted with model mesh sizes ranging from 0.1 to 1 mm. Specifically, simulations were performed with mesh sizes of 0.1, 0.2, 0.5, 0.8, and 1 mm, respectively. The results obtained from these simulations for samples No. 5 and No. 10 in Table 2, particularly focusing on the case where the mesh size is 0.2 mm, are presented in Figure 6. The present systematic analysis will therefore give a comprehensive grasp of variations in mesh size in the dynamic behavior and performance of the transducer for optimization within the numerical model for arriving at true and dependable forecasts. For these reasons, as compared with theoretical values concerning the resonance frequency, choosing a mesh size value of 0.2 mm is very reasonable. The resonant frequency of the vibrating structure from modal analysis was 19,180 Hz. This value deviates by a very small margin of 0.8% from the resonant frequency as determined by the analytical model, which was calculated to be 20,001 Hz. The agreement of the numerical and analytical results verifies that the finite element model is accurate enough to capture the dynamic behavior of the system. These results put into evidence the trend of how electrode material and thickness would impact the transducer performance due to interactions between mass and stiffness with geometric constraints. Inertia from additional material, for instance, can account for a decrease

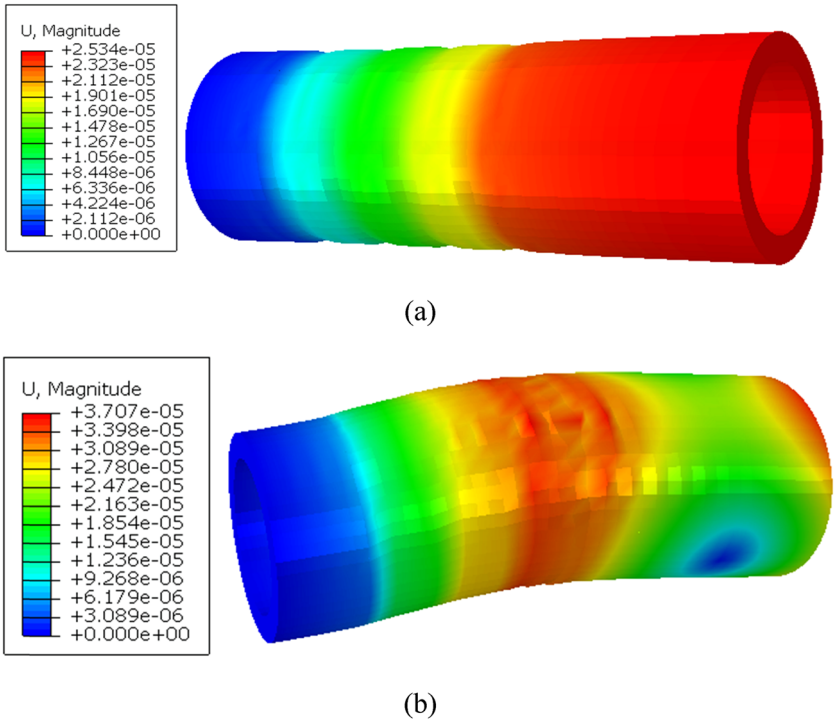

Figure 6: Vibration amplitude and first mode shape of the ultrasonic transducer: (a) sample No. 5 and (b) sample No. 10. Source: Created by the authors.

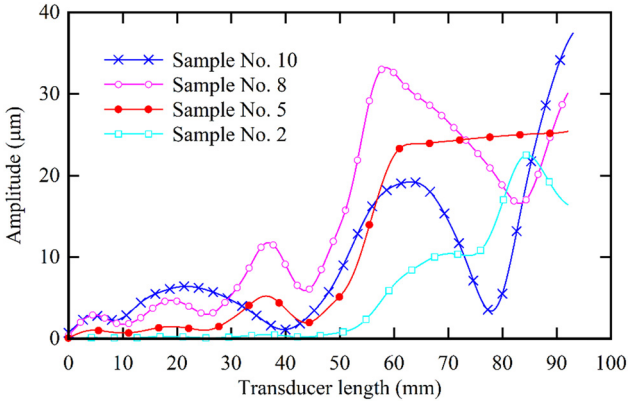

Figure 7: Finite element mode shape in four different configurations of the Langevin transducer for a voltage of 400 V. Source: Created by the authors.

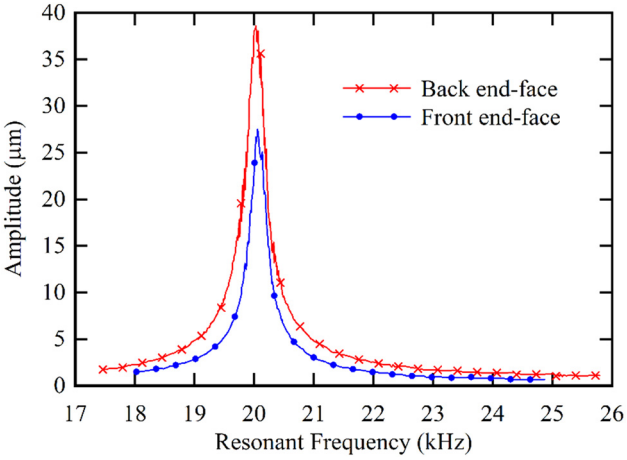

Figure 8: Frequency–response curve of front and back end-faces. Source: Created by the authors.

in natural frequency with increased electrode thickness. Similarly, the observation of aluminum electrodes yielding a smaller size of the transducer compared to copper can be related to the lower density and elastic modulus, allowing a greater degree of structural optimization. These findings underscore the importance of material selection in designing efficient and compact transducers, guided by a detailed understanding of the physical mechanisms underlying their behavior.

The vibration mode shape of the transducer is achieved using the finite element model at a voltage of 400 V. As depicted in Figure 7, the system of sample No. 10 exhibits three nodal points. The booster's nodal plane must align with the flange to prevent the transmission of oscillations to the welding machine structures. Additionally, this figure enables the calculation of the magnification factor for each component, providing valuable insights into their vibrational characteristics and distribution. The results reveal that for samples 2, 5, 8, and 10, the maximum range of longitudinal displacement of the transducer is 22.5, 25.4, 33.2, and 37.5 μm, respectively. Consequently, the maximum range of transducer No. 10 exceeds that of transducer No. 8 by approximately 10%. This comparison underscores the varying degrees of longitudinal displacement exhibited by different transducer samples, highlighting transducer No. 10 as the most pronounced in terms of displacement magnitude among the mentioned samples. Furthermore, it is evident that the shape of the vibration modes is strongly influenced by the configuration of the piezoelectric layers of the transducer, in addition to the maximum displacement. This underscores the importance of carefully examining the results of finite element simulations for the appropriate design of the transducer. By considering both the maximum displacement and the vibration mode shapes, engineers can ensure that the transducer is effectively designed to meet its intended performance requirements.

Using the electric-structure coupling model, a harmonic response simulation is applied to the ultrasonic transducer. The modal superposition method is employed for this harmonic response analysis. This analysis is performed to determine the amplification coefficient of the transducer. A 300 V alternating voltage is applied to the face of the PZT, and the resulting harmonic response curves are illustrated in Figure 8. This figure illustrates the displacement of the center point on both the front face and the back face. Under a driving voltage of 400 V, longitudinal displacement and transducer voltage were measured in a finite element model, and the results are presented in Figure 9. Notably, a distinct peak in displacement and sensor voltage emerged at a resonant frequency of 20 kHz. The observed sensor voltage closely mirrored the displacement, exhibiting a strong correlation between the two parameters. These findings indicate a robust relationship between the displacement and

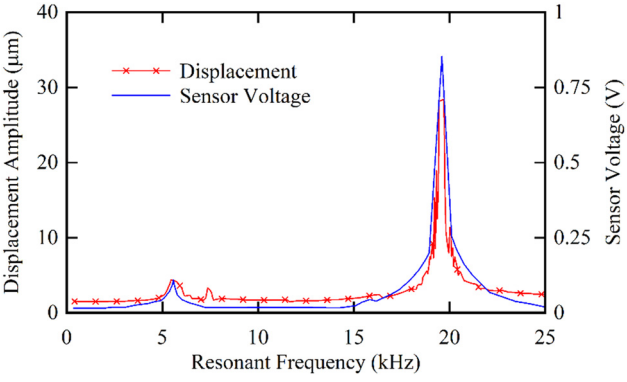

Figure 9: Frequency–response of sample No. 10 under a driving voltage of 400 V. Source: Created by the authors.

sensor voltage, confirming the sensor's capability to accurately reflect changes in displacement.

Simplifications made in the analytical model, such as disregarding wave reflections on the contact surfaces, can introduce errors in calculating the admittance and vibration amplitudes. Investigating the impact of voltage variations on the physical properties of piezoceramics constitutes a focus of our forthcoming research endeavors. This exploration aims to provide deeper insights into how changes in voltage influence the behavior of piezoceramic materials, thus enhancing the accuracy and reliability of our analytical predictions.

It is important to note that the conclusion regarding the optimality of aluminum electrodes in minimizing the size of the Langevin transducer is based solely on a comparative analysis between aluminum and copper. The observed advantage of aluminum stems from its lower density and elastic modulus, which contribute to reduced transducer dimensions while maintaining the desired natural frequency. However, this analysis does not account for the potential performance of other materials, such as titanium, magnesium alloys, or advanced composites, which may offer further optimization in size, efficiency, or other performance metrics. Future studies will extend this work by incorporating a broader range of materials to validate the findings presented here or identify alternative materials that could yield superior results.

4 Conclusion

In this study, the vibration behavior of the Langevin transducer was examined using the continuous theory of rods. Through this analysis, the impact of various parameters on the transducer's vibration characteristics was investigated. Additionally, a finite element model was incorporated into the study to further enhance the analysis. The research efforts culminated in determining the geometric specifications necessary to minimize the size of the transducer. The findings revealed that increasing the thickness of the electrode layers leads to a reduction in the natural frequency of the transducer. Specifically, as the thickness of the piezoelectric layers increased from 10 to 50 mm, the natural frequency decreased by approximately 27% for copper electrodes and 24% for aluminum electrodes. Notably, this frequency reduction was more pronounced for copper electrodes compared to aluminum electrodes. Moreover, with a thickness of 50 mm for the piezoelectric layers, the natural frequency of the transducer with copper electrodes was approximately 8.4% higher than that with aluminum electrodes. Additionally, increasing the thickness of the copper electrode from 0.3 to 2.0 mm resulted in a decrease of about 13 and 10% in the thickness of the backing and matching parts, respectively, along with a 1.7% reduction in the overall transducer length. The study concluded that utilizing aluminum electrodes in the Langevin transducer yielded the optimal size. Moving forward, these findings provide valuable insights into optimizing the design of Langevin transducers in future applications, especially with the incorporation of finite element modeling to further refine the analysis.

Building on this research, future work could involve real-world testing (experimental validation) of the designed transducers to confirm theoretical and simulation results. Additionally, exploring more complex beam models (like Rayleigh theory) for a more comprehensive analysis, and developing a multi-objective optimization framework that considers factors like size, efficiency, power output, and bandwidth tailored to specific applications could lead to even more refined miniaturized high-power Langevin transducers for various fields. This study demonstrates that aluminum electrodes yield a smaller transducer size compared to copper, primarily due to their lower density and elastic modulus. However, this conclusion is limited to the materials analyzed. Future work will explore additional materials to validate these findings and identify other potential options for further optimization.

Acknowledgments: The authors also gratefully acknowledge the support of Shenzhen Multi Field Precision Co .Ltd. which provided essential technical assistance and research resources throughout this study.

Funding information: This work was supported by the National Natural Science Foundation of China (No. 52365064 and No. 52365058), and Talents Revitalization for Inner Mongolia Project Team (2025TEL02).

Author contributions: All authors contributed to the conception and design of the study. Data collection, simulation, and analysis were performed by Yunhe Zou, Shufeng Tang, Yuezheng Lan, Tingting Zhang, and Shijie Guo. The first draft of the manuscript was written by Shufeng Tang, and all authors commented on previous versions of the manuscript. All authors have read and approved the manuscript.

Conflict of interest: The authors declare that there are no conflicts of interest.

Data availability statement: Not applicable.

References

Adachi K., Suzuki K., and Shibamata Y. (2018). "Stable operation of a high-power piezoelectric transformer comprising two identical bolt-clamped Langevin-type transducers and a stepped horn," Jpn. J. Appl. Phys., vol. 57, no. 6, p. 066701, DOI: https://doi.org/10.7567/JJAP.57.066701.

Alijani A. (2022). "The effect of magnetic field on buckling and nonlinear vibrations of Graphene nanosheets based on nonlocal elasticity theory," Int. J. Nano Dimens., vol. 13, no. 1, pp. 54–70, DOI: https://doi.org/10.22034/ijnd.2022.683988.

Baghal A. E. A., Maleki A., and Vafaei R. (2021). "On the pull-out behavior of hooked-end shape memory alloys fibers embedded in ultra-high performance concrete," Int. J. Eng. Technol. Innov., vol. 11, no. 4, pp. 265–277, DOI: https://doi.org/10.46604/ijeti.2021.7060.

Balali Dehkordi H. R. and Tadi Beni Y. (2024). "Size-dependent coupled bending-torsional analysis of piezoelectric micro beams," Mech. Based Des. Struct. Mach., vol. 52, no. 9, pp. 6484–6506, DOI: https://doi.org/10.1080/15397734.2023.2278674.

Beirami A. A. M., Ponkratov V. V., Baghal A. E. A., Abdullaeva B., and Nasrabadi M. (2023). "Cost-effectiveness dynamics and vibration of soft magnetoelastic plate near rectangular current-carrying conductors," Struct. Eng. Mech., vol. 88, no. 2, pp. 159–168, DOI: https://doi.org/10.12989/sem.2023.88.2.159.

Beni Y. T. (2022a). "Size dependent torsional electro-mechanical analysis of flexoelectric micro/nanotubes," Eur. J. Mech.-A/Solids, vol. 95, p. 104648, DOI: https://doi.org/10.1016/j.euromechsol.2022.104648.

Beni Y. T. (2022b). "Size dependent coupled electromechanical torsional analysis of porous FG flexoelectric micro/nanotubes," Mech. Syst. Signal. Process., vol. 178, p. 109281, DOI: https://doi.org/10.1016/j.ymssp.2022.109281.

Beni Z. T. and Beni Y. T. (2022). "Dynamic stability analysis of size-dependent viscoelastic/piezoelectric nano-beam," Int. J. Struct. Stab. Dyn., vol. 22, no. 5, p. 2250050, DOI: https://doi.org/10.1142/S021945542250050X.

Dehkordi M. F., Beni Y. T., Dashtaki P. M., and Vanani S. F. (2023). "Effect of flexoelectricity on the Pull-in instability of beam-type NEMS," Eng. Anal. Bound. Elem., vol. 155, pp. 87–107, DOI: https://doi.org/10.1016/j.enganabound.2023.05.051.

Esmaeili J. and Andalibi K. (2019). "Development of 3D Meso-Scale finite element model to study the mechanical behavior of steel microfiber-reinforced polymer concrete," Comput. Concr. Int. J., vol. 24, no. 5, pp. 413–422, DOI: https://doi.org/10.12989/cac.2019.24.5.413.

Esmaeili J., Andalibi K., Gencel O., Maleki F. K., and Maleki V. A. (2021). "Pull-out and bond-slip performance of steel fibers with various ends shapes embedded in polymer-modified concrete," Constr. Build. Mater., vol. 271, p. 121531, DOI: https://doi.org/10.1016/j.conbuildmat.2020.121531.

Esmaeili J., Romouzi V., Kasaei J., and Andalibi K. (2023). "An investigation of durability and the mechanical properties of ultra-high performance concrete (UHPC) modified with economical graphene oxide nano-sheets," J. Build. Eng., vol. 80, p. 107908, DOI: https://doi.org/10.1016/j.jobe.2023.107908.

Fallah M. and Arab Maleki V. (2021). "Piezoelectric energy harvesting using a porous beam under fluid-induced vibrations," Amirkabir J. Mech. Eng., vol. 53, no. 8, pp. 4633–4648, DOI: https://doi.org/10.22060/mej.2021.18200.6780.

Ghaderi M., Maleki V. A., and Andalibi K. (2015). "Retrofitting of unreinforced masonry walls under blast loading by FRP and spray on polyurea," Cumhur. Üniv. Fen Fak. Fen Bilimleri Derg., vol. 36, no. 4, pp. 462–477, DOI: https://doi.org/10.17776/CSJ.82511.

Ghobadi A., Beni Y. T., and Żur K. K. (2021). "Porosity distribution effect on stress, electric field and nonlinear vibration of functionally graded nanostructures with direct and inverse flexoelectric phenomenon," Compos. Struct., vol. 259, p. 113220, DOI: https://doi.org/10.1016/j.compstruct.2020.113220.

Gu G., Wu S., Wang D., Zhang B., Li C., and Liang Z. (2024). "Machining mechanism of metal glass cutting based on ultrasonic vibration tool path," Int. J. Adv. Manuf. Technol., vol. 131, no. 5, pp. 2967–2983, DOI: https://doi.org/10.1007/s00170-023-12818-8.

Jahanghiry R., Yahyazadeh R., Sharafkhani N., and Maleki V. A. (2016). "Stability analysis of FGM microgripper subjected to nonlinear electrostatic and temperature variation loadings," Sci. Eng. Compos. Mater., vol. 23, no. 2, pp. 199–207, DOI: https://doi.org/10.1515/secm-2014-0079.

Karafi M. and Kamali S. (2021). "A continuum electro-mechanical model of ultrasonic Langevin transducers to study its frequency response," Appl. Math. Model., vol. 92, pp. 44–62, DOI: https://doi.org/10.1016/j.apm.2020.11.006.

Khosravi S. and Amjadian M. (2024). "A parametric study on the energy dissipation capability of frictional mechanical metamaterials engineered for vibration isolation," in Active and Passive Smart Structures and Integrated Systems XVIII, SPIE, pp. 229–239, DOI: https://doi.org/10.1117/12.3010913.

Khosravi S., Amirsardari S., and Goudarzi M. A. (2025). "Dynamic behavior of rectangular tanks with limited freeboard under seismic loads: Experimental, analytical, and machine learning investigations," J. Press. Vessel. Technol., vol. 147, no. 2, p. 021901, DOI: https://doi.org/10.1115/1.4066967.

Khosravi S., Yousefi M. M., and Goudarzi M. (2021). "Development of seismic fragility curves of cylindrical concrete tanks using nonlinear analysis," Amirkabir J. Civ. Eng., vol. 53, no. 1, pp. 71–88, DOI: https://doi.org/10.22060/ceej.2021.19121.7079.

Li C., Zhu C. X., Zhang N., Sui S. H., and Zhao J. B. (2022a). "Free vibration of self-powered nanoribbons subjected to thermal-mechanical-electrical fields based on a nonlocal strain gradient theory," Appl. Math. Model., vol. 110, pp. 583–602, DOI: https://doi.org/10.1016/j.apm.2022.05.044.

Li G., Qu J., Xu L., Zhang X., and Gao X. (2022b). "Study on multi-frequency characteristics of a longitudinal ultrasonic transducer with stepped horn," Ultrasonics, vol. 121, p. 106683, DOI: https://doi.org/10.1016/j.ultras.2022.106683.

Li H. N., Wang W., Lai S. K., Yao L. Q., and Li C. (2024). "Nonlinear vibration and stability analysis of rotating functionally graded piezoelectric nanobeams," Int. J. Struct. Stab. Dyn., vol. 24, no. 9, p. 2450103, DOI: https://doi.org/10.1142/S0219455424501037.

Liu, Y., Nguyen, L. T. K., Li, X., and Feeney, A. (2024). "A Timoshenko-Ehrenfest beam model for simulating Langevin transducer dynamics," Appl. Math. Model., vol. 131, pp. 363–380, DOI: https://doi.org/10.1016/j.apm.2024.04.019.

Lu, X., Hu, J., Peng, H., and Wang, Y. (2017). "A new topological structure for the Langevin-type ultrasonic transducer," Ultrasonics, vol. 75, pp. 1–8, DOI: https://doi.org/10.1016/j.ultras.2016.11.008.

Ma X., Yang Y., Qiu J., Zhang J., Vasiljev P., Wu J., et al. (2024). "A novel rotary ultrasonic motor based on multiple Langevin transducers: Design, simulation, and experimental investigation," Smart Mater. Struct., vol. 33, no. 5, p. 055001, DOI: https://doi.org/10.1088/1361-665X/ad37b4.

Madinei H., Rezazadeh G., and Sharafkhani N. (2013). "Study of structural noise owing to nonlinear behavior of capacitive microphones,"

Microelectron. J., vol. 44, no. 12, pp. 1193–1200, DOI: https://doi.org/10.1016/j.mejo.2013.08.003.

Maleki V. A. and Mohammadi N. (2017). "Buckling analysis of cracked functionally graded material column with piezoelectric patches," Smart Mater. Struct., vol. 26, no. 3, p. 035031, DOI: https://doi.org/10.1088/1361-665X/aa5324.

Minaei M., Rezaee M., and Arab Maleki V. (2021). "Vibration analysis of viscoelastic carbon nanotube under electromagnetic fields based on the nonlocal Timoshenko beam theory," Iran. J. Mech. Eng. Trans. ISME, vol. 23, no. 2, pp. 176–198, DOI: https://doi.org/10.30506/ijmep.2020.115153.1639.

Patel L. K., Singh A. K., Sharma V., and Kala P. (2021). "Analysis of a hybrid ultrasonic horn profile using finite element analysis," Mater. Today Proc., vol. 41, pp. 772–779, DOI: https://doi.org/10.1016/j.matpr.2020.08.465.

Pérez-Sánchez, A., Segura, J. A., Rubio-Gonzalez, C., Baldenegro-Pérez, L. A., and Soto-Cajiga, J. A. (2020). "Numerical design and analysis of a Langevin power ultrasonic transducer for acoustic cavitation generation," Sens. Actuators A Phys., vol. 311, p. 112035, DOI: https://doi.org/10.1016/j.sna.2020.112035.

Piao C. and Kim J. O. (2017). "Vibration characteristics of an ultrasonic transducer of two piezoelectric discs," Ultrasonics, vol. 74, pp. 72–80, DOI: https://doi.org/10.1016/j.ultras.2016.09.021.

Pouraminian M., Akbari Baghal A. E., Andalibi K., Khosravi F., and Arab Maleki V. (2024). "Enhancing the pull-out behavior of ribbed steel bars in CNT-modified UHPFRC using recycled steel fibers from waste tires: a multiscale finite element study," Sci. Rep., vol. 14, no. 1, p. 19939, DOI: https://doi.org/10.1038/s41598-024-68682-3.

Pourreza T., Alijani A., Maleki V. A., and Kazemi A. (2021). "Nonlinear vibration of nanosheets subjected to electromagnetic fields and electrical current," Adv. Nano Res., vol. 10, no. 5, pp. 481–491, DOI: https://doi.org/10.12989/anr.2021.10.5.481.

Rao S. S. (2019). *Vibration of continuous systems*. John Wiley & Sons, Hoboken, New Jersey, U.S.

Rezaee M. and Maleki V. A. (2015). "An analytical solution for vibration analysis of carbon nanotube conveying viscose fluid embedded in visco-elastic medium," Proc. Inst. Mech. Eng. C. J. Mech Eng Sci., vol. 229, no. 4, pp. 644–650, DOI: https://doi.org/10.1177/0954406214538011.

Samani M. S. E. and Beni Y. T. (2018). "Size dependent thermo-mechanical buckling of the flexoelectric nanobeam," Mater. Res. Express, vol. 5, no. 8, p. 085018, DOI: https://doi.org/10.1088/2053-1591/aad2ca.

Sun D., Wang S., Hata S., and Shimokohbe A. (2010). "Axial vibration characteristics of a cylindrical, radially polarized piezoelectric transducer with different electrode patterns," Ultrasonics, vol. 50, no. 3, pp. 403–410, DOI: https://doi.org/10.1016/j.ultras.2009.09.008.

Tadi Beni Y. (2016). "Size-dependent electromechanical bending, buckling, and free vibration analysis of functionally graded piezoelectric nanobeams," J. Intell. Mater. Syst. Struct., vol. 27, no. 16, pp. 2199–2215, DOI: https://doi.org/10.1177/1045389X15624798.

Vjuginova, A. A. (2019). "Multifrequency Langevin-type ultrasonic transducer," Russ. J. Nondestr. Test., vol. 55, pp. 249–254, DOI: https://doi.org/10.1134/S1061830919040132.

Wang L., Hofmann V., Bai F., Jin J., and Twiefel J. (2019). "A novel additive manufactured three-dimensional piezoelectric transducer: Systematic modeling and experimental validation," Mech. Syst. Signal. Process, vol. 114, pp. 346–365, DOI: https://doi.org/10.1016/j.ymssp.2018.05.025.

Wang X., Wang G., Chen Z., Lim C. W., Li S., and Li C. (2024). "Controllable flexural wave in laminated metabeam with embedded multiple resonators," J. Sound. Vib., vol. 581, p. 118386, DOI: https://doi.org/10.1016/j.jsv.2024.118386.

Wang X., Zhang X., Shi L., Wu C., and Chen G. (2023). "Enhancing heat and mass transfer to suppress void defects in friction stir welding by superimposing ultrasonic vibration," Arch. Civ. Mech. Eng., vol. 23, no. 4, p. 256, DOI: https://doi.org/10.1007/s43452-023-00799-0.

Wellendorf A., von Damnitz L., Nuri A. W., Anders D., and Trampnau S. (2024). "Determination of the temperature-dependent resonance behavior of ultrasonic transducers using the finite-element method," J. Vib. Eng. Technol., vol. 12, no. 2, pp. 1277–1290, DOI: https://doi.org/10.1007/s42417-023-00906-8.

Wu J., Mizuno Y., and Nakamura K. (2018). "Vibration characteristics of polymer-based Langevin transducers," Smart Mater. Struct., vol. 27, no. 9, p. 095013, DOI: https://doi.org/10.1088/1361-665X/aad530.

Xie Z. Y., Guo L. M., Li C., Shi Y. T., and Han B. (2024). "Modeling the deformation of thin-walled circular tubes filled with metallic foam under two lateral loading patterns," Structures, vol. 69, p. 107289, DOI: https://doi.org/10.1016/j.istruc.2024.107289.

Yuan Z., Xiang D., Peng P., Zhang Z., Li B., Ma M., et al. (2023). "A comprehensive review of advances in ultrasonic vibration machining on SiCp/Al composites," J. Mater. Res. Technol., vol. 24, pp. 6665–6698, DOI: https://doi.org/10.1016/j.jmrt.2023.04.245.

Zhang Q., Shi S., and Chen W. (2016). "An electromechanical coupling model of a bending vibration type piezoelectric ultrasonic transducer," Ultrasonics, vol. 66, pp. 18–26, DOI: https://doi.org/10.1016/j.ultras.2015.11.013.

Zhao Q., Guo X., Wang H., Yin S., Kang R., Dong Z., et al. (2023). "Effects of ultrasonic vibration cutting trajectories on chip formation of tungsten alloys," J. Manuf. Process., vol. 92, pp. 147–156, DOI: https://doi.org/10.1016/j.jmapro.2023.02.053.

Zheng J., Liang K., Lin Z., Di H., and Cheng Y. (2023). "Double-armed cone-shaped flexoelectric transducer," Front. Phys., vol. 10, p. 1117705, DOI: https://doi.org/10.3389/fphy.2022.1117705.